Coatings **2015**, *5*, 263-277; doi:10.3390/coatings5030263

OPEN ACCESS

coatings

ISSN 2079-6412

www.mdpi.com/journal/coatings

Article

Trap Generation Dynamics in Photo-Oxidised DEH Doped Polymers

David M. Goldie

Division of Physics, University of Dundee, Perth Road, Dundee DD1 4HN, UK;
E-Mail: d.m.goldie@dundee.ac.uk; Tel.: +44-1382-384571; Fax: +44-1382-384389

Academic Editor: Alessandro Lavacchi

Received: 27 May 2015 / Accepted: 29 June 2015 / Published: 3 July 2015

Abstract: A series of polyester films doped with a hole transport molecule, p-diethylaminobenzaldehyde-1,1'-diphenylhydrazone (DEH), have been systematically exposed to ultraviolet radiation with a peak wavelength of about 375 nm. The electronic performance of the films, evaluated using time-of-flight and space-charge current injection methods, is observed to continuously degrade with increasing ultraviolet exposure. The degradation is attributed to photo cyclic oxidation of DEH that results in the creation of indazole (IND) molecules which function as bulk hole traps. A proposed model for the generation dynamics of the IND traps is capable of describing both the reduction in current injection and the associated time-of-flight hole mobility provided around 1% of the DEH population produce highly reactive photo-excited states which are completely converted to indazole during the UV exposure period. The rapid reaction of these states is incompatible with bulk oxygen diffusion-reaction kinetics within the films and is attributed to the creation of excited states within the reaction radius of soluble oxygen. It is suggested that encapsulation strategies to preserve the electronic integrity of the films should accordingly focus upon limiting the critical supply of oxygen for photo cyclic reaction.

Keywords: DEH; photo-oxidation; indazole; traps

1. Introduction

The use of polymers in plastic electronic devices is becoming increasingly significant for the development of many new commercial products in the display, sensor and smart labeling markets. Although there are many attractive benefits offered by a plastic electronics implementation such as

process simplicity and reduced manufacture costs [1–3] a principal drawback, which must frequently be addressed by the organic electronics community, is the degradation of electronic performance in a proposed device configuration. Degradation phenomena are commonly manifested through prolonged device operation under normal ambient conditions and often involve irreversible oxidation processes that are initiated via molecular excitation. Considerable technological effort has therefore focused either upon chemical modification of the active polymer to improve stability, or more robust encapsulation of plastic devices which are deployed under normal environmental conditions [4]. Whilst such strategies have generally improved the operational lifetime of plastic electronic products to fulfill acceptable commercial benchmarks there remain many optoelectronic applications where alternative measures to minimise residual degradation artifacts must be sought. Under these circumstances it is important to have a comprehensive understanding of the fundamental photo-oxidation mechanisms and in particular what are the key operational parameters that dictate the generation rate of oxidation products.

A convenient class of materials in which to systematically study such photo-oxidation processes are molecularly doped polymers (MDPs). These comprise a host polymer, such as polycarbonate, polyester or polystyrene, into which are added controlled amounts of a small dopant molecule (typically hydrazones, amines or thiophenes). Under appropriate excitation a proportion of the dopant molecules may be stimulated and a unipolar hole current may then be induced to flow through the MDP via a sequence of reduction-oxidation reactions when an external electric field is applied. Thin films of such MDPs are commonly used by the xerographic, laser printer and organic LED display industries [5]. An interesting class of MDPs that have received considerable attention in the scientific literature are those based upon hydrazone molecules and in particular p-diethylaminobenzaldehyde-1,1'-diphenylhydrazone (DEH) [6–10]. The DEH molecule also exhibits a unique photo-cyclic oxidation reaction which results in the production of an indazole molecule 1-phenyl-3-(4-diethylamino-1-phenyl)-1,3-indazole (IND) [11,12]. Efficient conversion of DEH to IND requires exposure to UV irradiation and the presence of molecular oxygen; no IND is produced for UV exposure of pure DEH under vacuum conditions.

The significance of the production of IND molecules for hole transport in DEH MDPs has to date received relatively little attention with the exception of a study for a polycarbonate host where a modest decrease of hole mobility was recorded under prolonged ultraviolet (UV) exposure [13]. The present work seeks to extend knowledge concerning the photo-oxidation of DEH using a complementary polyester based MDP. Systematic monitoring of both the hole mobility and the achieved hole injection current into such MDP films under progressive UV exposure is used to deduce the underlying dynamics of IND production. Knowledge of the IND generation dynamics is subsequently used to identify and evaluate the key parameters that control the rate of DEH photo-oxidation and inform appropriate tactics to subvert the degradation of electronic performance.

2. Experimental Section

To provide a convenient source of hole carriers for time-of-flight (TOF) and space-charge-limited current (SCLC) injection measurements [5] the DEH MDP films were deposited onto aluminised Melinex substrates that were pre-coated with a 0.36 μm thick charge-generation (CG) layer. The CG layer comprised a 50% by weight dispersion of x-form metal free phthalocyannine (x-H_2Pc) in a commercial polyester resin (Vitel 2200) which has a similar structure to poly(ethylene terepthalate) (PET). The CG

was applied to the substrates using a mechanised wire bar coating unit from a butan-2-one:toluene solution in which the Vitel and x-H_2Pc constituents were successively dissolved by ball milling with glass beads. Following a drying period of one hour at 90 °C the CG layer was then over coated with the MDP layer which comprised a 50% by weight solution of DEH to the Vitel polyester. The thickness (L) of the MDP layers, which were also wire bar coated using dichloromethane:toluene solutions, was 6.5 μm following a similar drying period for the CG layer. The x-H_2Pc, DEH and Vitel materials were all sourced from industrial suppliers and used without further purification.

Photo-oxidation of the DEH MDP layer was performed by illuminating the exposed surfaces of identically prepared specimens to varying amounts of UV radiation from a commercially available 3.6 mW LED. The spectral output of the LED source peaked at 375 nm (spectral width ~±18 nm) and resulted in an estimated photon flux of around 7×10^{15} s^{-1} across the illuminated MDP surface. The selected exposure wavelength ensured that all UV absorption processes occurred within the DEH dopant molecules [13] as the polyester absorption edge is located at a deeper UV wavelength of about 325 nm [14,15]. UV induced degradation of the polyester binder itself, and the associated generation of contaminating chemical by-products which might complicate subsequent data interpretation, is consequently avoided. Absorption of the UV radiation is furthermore calculated to be entirely confined within the MDP layer thickness for the measured DEH absorption coefficient at 375 nm ($\alpha_0 = 5 \times 10^4$ cm^{-1}). Possible degradation of the photogeneration efficiency of the CG layer is therefore also avoided at the selected UV exposure wavelength which is important for the correct interpretation of the observed SCLC data trends. UV exposure times ranging from 72 s to 67 h were applied, with perceptible darkening of the films being observed for the longest exposures. Following the exposure period a thin semi-transparent layer of aluminium was deposited onto the MDP surface by thermal vacuum evaporation to form capacitive structures (Al/CG/MDP/Al), which could be electronically tested.

For the TOF and SCLC testing of the UV exposed samples hole carriers were photo-generated in the CG layer for subsequent injection into the MDP. Visible red light from a commercially available LED (3000 mcd intensity; 660 nm peak spectral response) was focused through the top semi-transparent Al contact (transmission at 660 nm between 12% and 18%) and absorbed within the CG layer. For TOF measurements the LED output was pulsed for 10 μs to ensure that small-signal conditions pertained whereby the amount of CG charge (Q_{CG}) was attenuated so that $Q_{CG} < 0.1\ CV$ where C represented the capacitance of the samples (~160 pF) and V the externally applied voltage across the Al contacts. Transient signals generated under such TOF photo-excitation were digitally captured on a storage oscilloscope following signal averaging before being transferred to a computer for analysis to determine the hole mobility (μ). By contrast SCLC measurements were performed by fast-switching of the LED to a permanently on-state under significantly higher intensity conditions ($Q_{CG} > CV$). For SCLC measurements signals were similarly digitised to determine the injected current density (J) but acquired in a single-shot mode to avoid the possibility of charge accumulation in the MDP layer and associated hysteresis effects. A low repetition rate (<0.03 Hz) for LED illumination further ensured that any remaining bulk charge was removed between successive SCLC injection events. A stabilised high voltage power supply was used for both the TOF and SCLC measurements to record signals for 10 V < V < 450 V. All UV exposure and electronic measurements were conducted under ambient conditions at a fixed temperature of 295 K.

3. Results and Discussion

The experimental data recorded by the TOF and SCLC measurements are summarised in Figures 1 and 2, respectively.

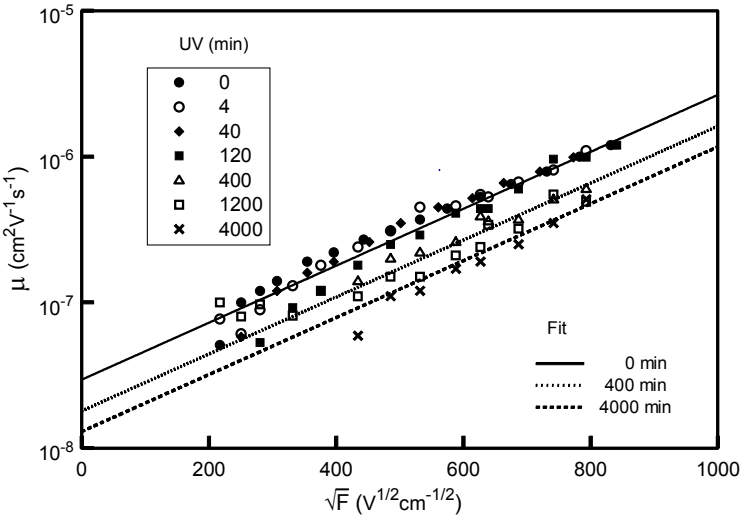

Figure 1. Hole mobility data recorded for a series of DEH MDP films that have been subjected to the UV exposure periods indicated. The solid lines show the optimised fit of Equation (1) to selected samples using adjustable values of μ_0.

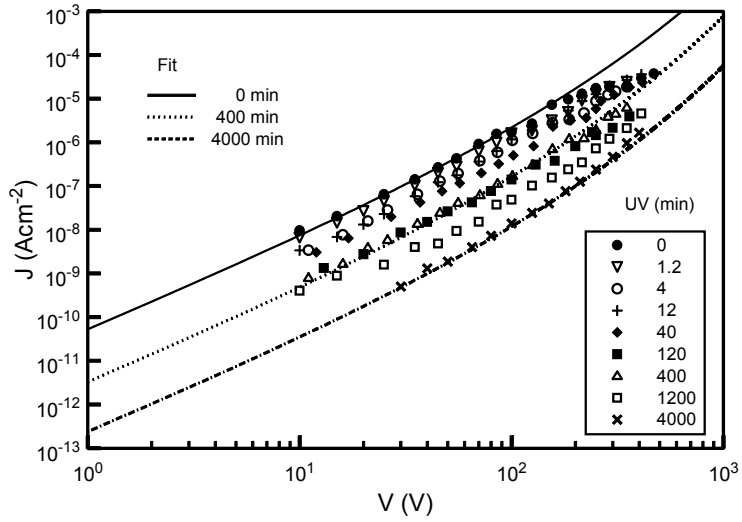

Figure 2. SCLC *J*(*V*) data recorded for a series of DEH MDP films that have been subjected to the UV exposure periods indicated. The solid lines show the optimised fit of Equation (3) for selected UV exposures: 400 min, θ = 0.15; 4000 min, θ = 0.015.

The TOF mobility data are observed to be consistent with Poole-Frenkel type behaviour that is characteristic of hopping transport in MDPs such that [16,17]:

$$\mu = \mu_0 \exp\left(\beta_{PF}\sqrt{F}\right) \quad (1)$$

In Equation (1), F (= V/L) represents the static electric field across the MDP layer, and β_{PF} depends upon the energetic and positional disorder that are associated with the MDP compositional landscape through which hole carriers hop [5]. For electric fields lower than about 9×10^4 V·cm^{-1} the mobility values are observed to increasingly deviate from data fitted to Equation (1) at higher fields. This phenomenon is attributed to delayed hole injection across the CG-MDP interface and these low field mobility data have consequently been ignored when applying Equation (1) to determine how μ_0 and β evolve with UV exposure. It is then evident from Figure 1 that by increasing the UV exposure the zero-field mobility μ_0 is slowly reduced but this does not appear to be accompanied by a systematic change in β_{PF}. Similar behaviour has previously been reported for DEH doped polycarbonate films [13] with the μ_0 reduction being attributed to the progressive reduction of available hopping states in the highest occupied molecular orbital (HOMO) of the DEH molecule. Dilution of HOMO states results in an increase in the average hole hopping distance (ρ) and a diminished wavefunction overlap probability so that for a characteristic DEH localisation length (ρ_0) [6,18]:

$$\mu_0 \propto \rho^2 \exp\left(-\frac{2\rho}{\rho_0}\right) \tag{2}$$

The effect of UV exposure is also apparent in the SCLC data which show a continuous reduction of the $J(V)$ response as the exposure period is increased. For MDP hopping transport characterised by Equation (1) the associated $J(V)$ response may then be approximated by [19]:

$$J = \theta \frac{9}{8} \frac{\varepsilon \mu V^2}{L^3} \tag{3}$$

In Equation (3), ε represents the permittivity of the MDP and θ denotes a constant (≤ 1) whose magnitude reflects departures from the maximum space-charge injection current due to the presence of traps. Under steady-state trap-limited hopping conditions where the density (N_t) of iso-energetic traps remains non-saturated, the magnitude of θ is given by:

$$\theta = \frac{1}{\left[1 + N_t\left(\frac{C_t}{R_l}\right)\right]} \tag{4}$$

The quantities C_t and R_l in Equation (4) respectively denote the volume capture rate and release rate of holes between the trapping centres and the DEH HOMO. Assuming that C_t and R_l represent well-defined quantities that are characteristic of the fundamental chemical nature of the trap, the trap concentration N_t may consequently be deduced from Equation (4) by noting the relative reduction in SCLC current response relative to the trap-free ($N_t = 0$, $\theta = 1$) $J(V)$ reference.

A consistent interpretation of both the TOF and SCLC data thus emerges if under UV exposure a proportion of the DEH dopant molecules in the MDP layer are converted to a different chemical species which function as hole traps. The progressive conversion of DEH as the UV exposure period is increased provides the necessary dilution effect to account for the observed μ_0 reduction via Equation (2), whilst the accompanying decrease of SCLC $J(V)$ data may be explained via Equation (3) and (4) through the associated creation of traps. The proposed chemical conversion mechanism involves the photo-cyclic

oxidation of DEH to form IND molecules [11] which function as hole traps according to the scheme depicted in Figure 3.

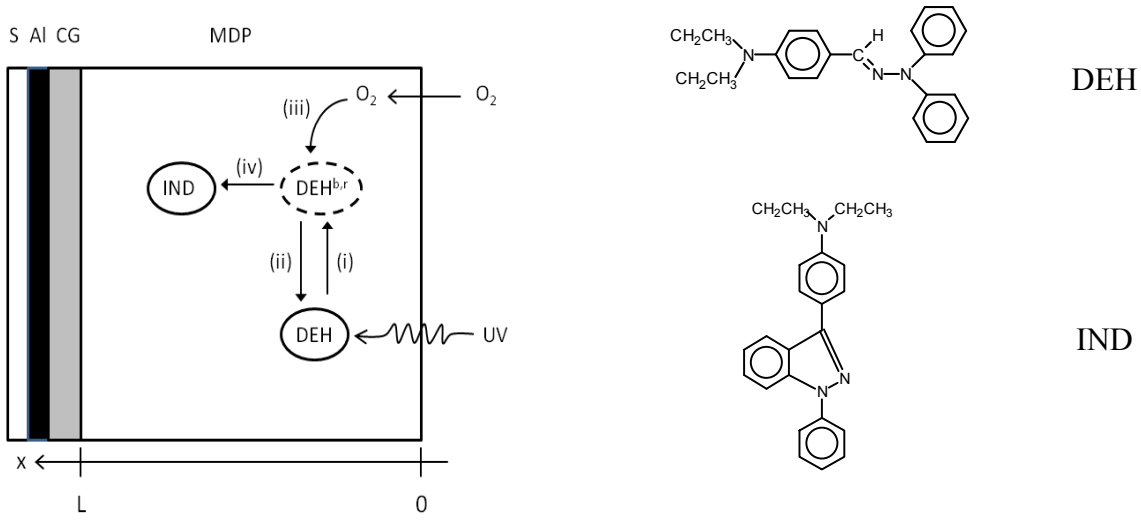

Figure 3. Photo-cyclic oxidation model for DEH MDP film structures according to processes (i)–(iv) described in the text. The chemical structures of the DEH and IND molecules are indicated. S = substrate.

The conversion of DEH to IND involves several processes, which are labeled (i)–(iv) in Figure 3 and may be summarised as follows:

1. absorption of UV photons by DEH to either form: (a) bulk excited states (DEH^b) which may relax back to DEH before reaction with oxygen; (b) reactive excited states (DEH^r) which are created close to soluble oxygen and rapidly react to form indazole molecules.
2. relaxation of un-reacted DEH^b states to DEH
3. diffusion of soluble oxygen within reaction radius of DEH^b.
4. reaction of soluble oxygen with DEH^b to form indazole molecules

The time (t) dynamics of these internal processes may be concisely incorporated into a set of coupled partial differential rate equations for the volume concentrations of DEH (M), DEH^b (B), DEH^r (R), oxygen (C) and bulk indazole (I). For uniform UV exposure across the film surface, these concentrations are only expected to vary one-dimensionally (x) along the normal axis between the film surface ($x = 0$) and $x = L$ so that:

$$\frac{\partial M}{\partial t} = -GM + \beta B \tag{5a}$$

$$\frac{\partial B}{\partial t} = GM\left(1-\varphi\right) - 4\pi\rho_R D\left(BC\right) - \beta B \tag{5b}$$

$$\frac{\partial R}{\partial t} = GM\varphi \tag{5c}$$

$$\frac{\partial C}{\partial t} = D\frac{\partial^2 C}{\partial x^2} - 4\pi\rho_R D\left(BC\right) - GM\varphi \tag{5d}$$

$$\frac{\partial I}{\partial t} = 4\pi\rho_R D(BC) \tag{5e}$$

In the above rate equations φ represents the proportion of DEH molecules which form reactive DEH^r states upon UV absorption, β gives the relaxation rate of un-reacted DEH^b to DEH, D is the diffusion coefficient for soluble oxygen, ρ_R denotes the reaction radius for DEH^b, and G gives the UV photo-generation rate of DEH to the excited $DEH^{b,r}$ states. An appropriate model for G is complicated by the presence of the MDP polymer binder but is expected to be proportional to the incident UV intensity (G_{UV}), and also to depend upon the local instantaneous DEH absorption coefficient α(*x*,*t*). A possible form for α(*x*,*t*) might reasonably assume that, compared to the absorption coefficient α_0 prior to UV exposure, $\alpha(x,t) = \alpha_0\left[M(x,t)/M_0\right]^\gamma$ where M_0 is the initial DEH concentration and γ is an adjustable parameter. The photo-generation rate *G*(*x*, *t*) in Equation (5) is accordingly represented as:

$$G = G_{UV} e^{-\alpha_0\left(\frac{M(x,t)}{M_0}\right)^\gamma x} \tag{6}$$

The solution of the coupled rate equations, using Equation (6), may then proceed subject to appropriate initial conditions [$M(x,0) = M_0$; $B(x,0) = 0$; $R(x,0) = 0$, $I(x,0) = 0$; $C(x,0)$ = MDP oxygen solubility limit C_{sol}] and the boundary condition $C(0,t)$ = atmospheric oxygen concentration. Many of the rate equation parameters are either determined experimentally (G_{UV}, α_0, M_0), or may be estimated from known literature values (D, ρ_R, C_{sol}). A relatively small number of parameters (φ, β, γ and (R_I/C_t)) are therefore in practice available to fit the generated trap generation dynamics to the TOF and SCLC data. To investigate whether the modeled dynamics are capable of providing an acceptable fit to both data sets using a consistent set of parameters, an analysis strategy that focuses upon the total indazole concentration IND(*t*) was adopted. At any time during UV exposure IND(*t*) may be determined using the separate reaction contributions from DEH^b states (Equation (5e)) and DEH^r states (Equation (5c) where all DEH^r states are assumed to react with oxygen to produce indazole) so that:

$$IND(t) = \int_0^L I(x,t)\mathrm{d}x + \int_0^L R(x,t)\mathrm{d}x \tag{7}$$

Such a strategy proposes that IND(*t*) may then be used to determine both the total concentration of generated traps ($N_t(t)$ = IND(*t*)) and the remaining concentration of un-reacted DEH sites *M*(*t*) that are available for hole hopping ($M(t) = M_0$ – IND(*t*)). However, the simple use of IND(*t*) to permit these calculations demands that two important assumptions are fulfilled. It should first be noted that the rate equation model involves DEH^b states and thus at any time during UV exposure there will also exist total populations $B(t) = \int_0^L B(x,t)\mathrm{d}x$ and $M(t) = \int_0^L M(x,t)\mathrm{d}x$ so that for overall bulk molecular conservation $M_0 = M(t) + B(t) + I(t) + R(t)$. Under experimental conditions a population of states *B*(*t*) will consequently exist when UV exposure is terminated ($G = 0$) and these may either relax back to DEH states, or react with oxygen to form IND according to Equation (5e). For IND(*t*) to accurately represent the total bulk IND concentration no further DEH^b reactions should therefore occur after UV exposure has been terminated which demands that the relaxation rate β is significantly greater than the oxygen reaction rate $4\pi\rho_R DC$. The further assumption that must be addressed is whether the use of total bulk

quantities IND(t) and $M(t)$ is appropriate to model the experimental data given that implicit spatial variations exist across the film thickness due to the fundamental nature of the UV absorption process (Equation (6)). Previous TOF work [13] has endeavored to achieve a homogeneous distribution of IND throughout the film bulk by applying a post-exposure annealing procedure but this was not possible in the present work due to the use of Melinex substrates. Redistribution of IND throughout the film bulk by diffusion may nevertheless be inadvertently accomplished in the present case due to elevation of the film surface during thermal evaporation of the final encapsulating aluminium contacts. Further support for the applicability of bulk IND(t) and $M(t)$ model results to the present experimental data is provided through calculation of SCLC $J(V)$ characteristics which indicate that trapping becomes significantly less effective (with $\theta \rightarrow 1$) if the total concentration of generated traps become confined to an increasingly narrow region in the vicinity of $x = 0$ where UV absorption is strongest.

An illustrative set of normalised dynamical curves for $M(t)$, $B(t)$, $I(t)$ and $R(t)$ is given in Figure 4 using experimentally determined values for $G_{UV} = 4 \times 10^{-2}$ s^{-1}, $\alpha_0 = 5 \times 10^4$ cm^{-1}, $M_0 = 1 \times 10^{21}$ cm^{-3}, $\rho_R = 4 \times 10^{-8}$ cm ($\cong$ molecular radius of DEH), and selected parameter values $\varphi = 0.01$, $\beta = 0.01$, $\gamma = 1$, and a relaxation to reaction ratio ε ($=\beta/4\pi\rho_R DC(x,0)$) $= 2.5 \times 10^6$.

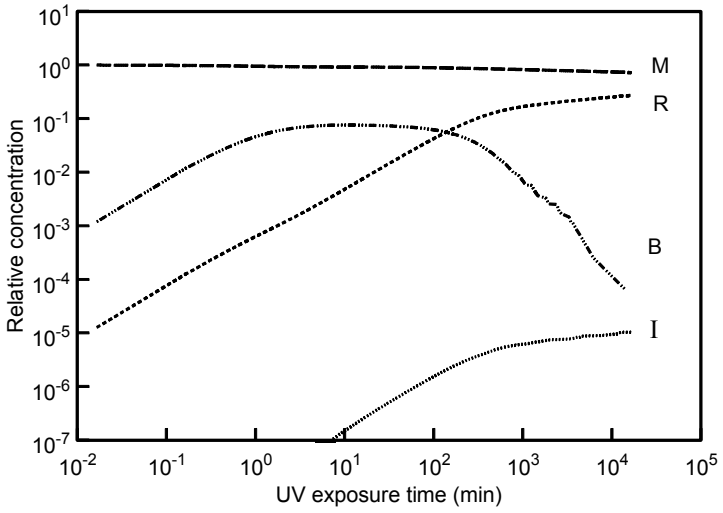

Figure 4. Modeled dynamics of DEH photo-oxidation with UV exposure for $\varphi = 0.01$, $\beta = 0.01$ and $\varepsilon = 2.5 \times 10^6$. The output concentrations are normalised to the initial DEH concentration M_0.

From the dynamical output it is observed that the anticipated reduction in $M(t)$ is accompanied by an increase of indazole from both $I(t)$ and $R(t)$ routes with $R(t)$ providing the dominant contribution to overall IND(t) production for the selected magnitude of φ. The rate of increase of $I(t)$ depends upon the available supply of DEH^b states and is approximately linear over the exposure interval (10^0 min $< t < 10^2$ min), where $B(t)$ remains fairly constant, before approaching a final saturated value when B(t) becomes depleted. The interval over which $B(t)$ remains approximately constant, and hence $I(t)$ increases linearly from Equation (5e), may be extended by increasing the relaxation to reaction ratio ε. Spreading the availability of DEH^b states across a longer exposure interval via relaxation control is accompanied by a smaller overall conversion to IND traps for equivalent overall exposure times. The dynamical output shown in Figure 4 suggests that a final equilibrium situation will only be attained for very long exposure periods when $I + R = M_0$, $M = 0$ and $B = 0$.

The influence of γ from Equation (6) upon the dynamics was found to be insignificant for $0 \le \gamma \le 1$ and for convenience was accordingly fixed at unity in all subsequent analysis. The only adjustable parameters that are available to control the dynamical output are therefore ε and φ. Initial estimates for these parameters may be obtained by considering how the hopping distance ρ(*t*) increases as the average DEH concentration *M*(*t*) diminishes with UV exposure, and using ρ(*t*) to fit the experimental variation of μ_0 observed in the TOF results (Figure 1). Using a cubic lattice approximation [6] ρ(*t*) may be calculated from IND(*t*) as:

$$\rho(t) = \left[\frac{M_w}{dA_v C_w \left(1 - \frac{IND(t)}{M_0} \right)} \right]^{\frac{1}{3}} \tag{8}$$

In Equation (8), M_w is the DEH molecular weight (343g), *d* is the DEH density (1.12 g·cm^{-3}), A_v is Avogadro's constant and C_w (=0.5) is the concentration by weight of DEH to polymer. Using $\rho_0 = 1.6 \times 10^{-8}$ cm for the DEH localisation length [20] the variation of μ_0 may thus be found using Equation (2), Equation (8) and generated IND(*t*) dynamics from Equation (7). To assist in the determination of an estimate for φ it is initially useful to consider that IND(*t*) is dominated by the *R*(*x*, *t*) integral term in Equation (7) for which a spatially-averaged analytical expression *R*(*t*) may obtained from Equation 5c by letting $M = (M_0 - R)$ and setting the spatial average of *G*(*x*, *t*) in Equation (6) to $\overline{G} = G_{UV} / \alpha_0 L$. From Equation (5c) it is then found that:

$$IND(t) = R(t) = M_0 \left[1 - e^{-\overline{G}\varphi t} \right] \tag{9}$$

The increase of IND(*t*) under these circumstances is expected to be linear in time for short UV exposure periods such that $t < \left(\overline{G}\phi\right)^{-1}$ so that by using Equation (9) in Equation (8) ρ(*t*) has a similar linear dependence with $\rho(t) \approx \rho(t=0)\left[1 + \frac{1}{3}\overline{G}\varphi t \right]$. The use of this approximate ρ(*t*) expression in Equation (2) finally permits an initial estimate for φ to be obtained. Results generated by this procedure are presented in Figure 5 where the μ_0 data are plotted in a normalised format relative to the zero-field mobility magnitude for a reference un-exposed sample.

The model curves shown in Figure 5 suggest that acceptable fitting of μ_0 requires that $\varphi \approx 0.01 \pm 0.005$ and $7.5 \times 10^5 < \varepsilon < 2.5 \times 10^7$ with an optimum $\varepsilon \approx 2.5 \times 10^6$. The influence of the selected magnitude of φ is illustrated in Figure 5 for the extreme limits where for φ = 0 (zero highly reactive states) the rate of IND production via purely DEH^b diffusive oxygen reactions *I*(*t*) is undetectable, whereas for φ =1 (entirely highly reactive DEH^r states) the IND generation rate should be detectable at much shorter exposure periods.

The associated IND(*t*) trap generation dynamics are plotted in Figure 6 using the corresponding φ and ε values that are inferred from the μ_0 analysis. The experimental trap densities deduced by applying Equation (3) and Equation (4) to the Figure 2 SCLC data are shown as symbols in Figure 6 using an adjustable scaling factor equal to (R_l/C_t). In practice Equation (3) was restricted to fitting *J*(*V*) data for *V* < 250 V since there was evidence that the CG layer was unable to meet the SCLC ohmic demands for higher current densities in samples subjected to the lowest UV exposure.

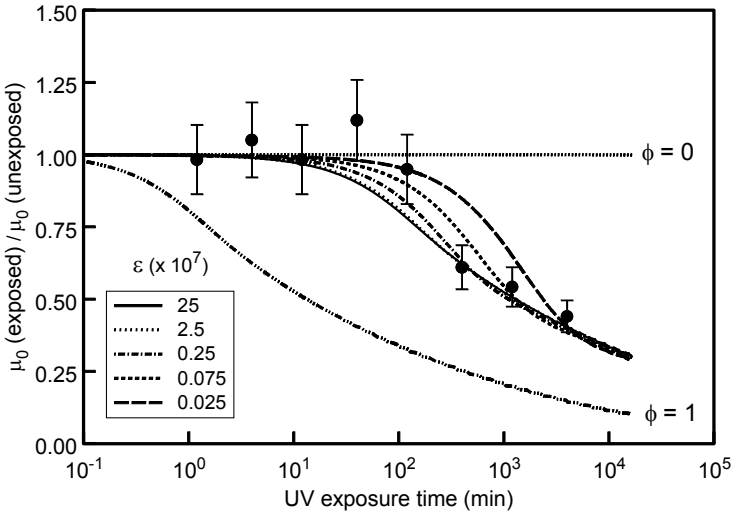

Figure 5. Variation of experimentally measured μ_0 with UV exposure period. The solid curves show the expected dependence based upon the modeled DEH photo-oxidation dynamics for the ε values given. φ = 0.01 in all cases except for those labeled.

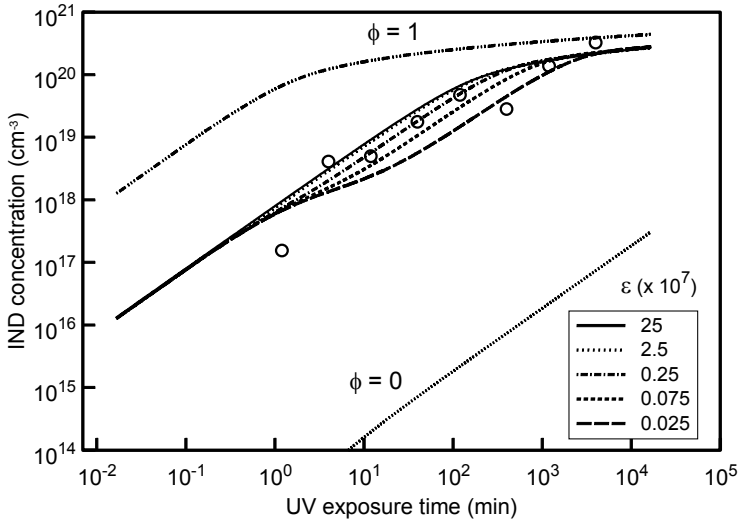

Figure 6. Variation of experimentally deduced IND trap concentrations with UV exposure period setting $(R_l/C_t) = 5 \times 10^{18}$ cm^{-3}. The solid curves show the expected dependence based upon the modeled DEH photo-oxidation dynamics for the ε values given. φ = 0.01 in all cases except for those labeled.

From Figure 6 it is found that the data points cannot in general be fitted by a linear dependence of N_t (corresponding to higher ε values) across the entire range of UV exposures but are better described by the N_t curves that correspond to the lower ε magnitudes as found by the μ_0 fitting procedure. Optimum agreement using $\varepsilon = 2.5 \times 10^6$ from the μ_0 analysis requires that $(R_l/C_t) = 5 \times 10^{18}$ cm^{-3} for the IND traps. No further information may presently be deduced concerning the individual magnitudes of R_l or C_t for the traps although it should in principle be possible to determine these values (subject to their ratio constraint) by simulating the temporal shape of the underlying TOF photocurrent and SCLC injection responses [5,21]. Given that the mobility reduction would appear to be entirely attributable to an increase

of ρ(*t*) via hopping state dilution, however, the traps must be relatively deep such that they do not engage in multiple trapping-and-release events with DEH HOMO states during a typical hole transit time. This implies that the inverse release rate $(R_l)^{-1}$ should be significantly less than the maximum hole transit-time across the MDP film thickness. For samples that have maximum UV exposure and are subject to the lowest experimental applied voltages the longest recorded transit times are found to be ~0.2 s so that $R_l << 5s^{-1}$. The loss of hole carriers to IND traps under these circumstances should result in the TOF pre-extraction current signals decreasing more rapidly as N_t increases, with the post-extraction currents displaying a weaker decay as trapped charge is eventually released and collected. These TOF trapping signatures are indeed evident in the normalised TOF current-time data presented in Figure 7.

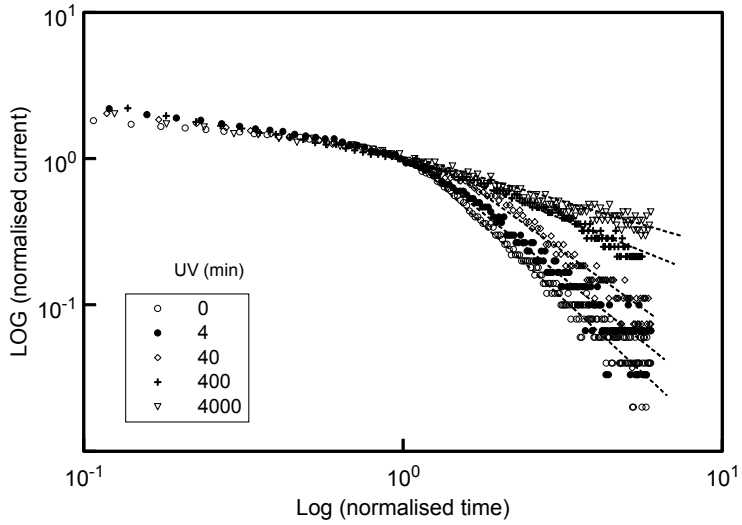

Figure 7. TOF current-time signals recorded at V = 250 V for a series of DEH MDP films that have been subjected to the UV exposure periods indicated. The signals have been normalised to the observed hole transit-times, and corresponding currents at these transit-times, to facilitate shape comparisons. The dashed lines are an aid for the eye in the post transit-time region.

An essential requirement for the conversion of DEH to IND is the available supply of oxygen. As already noted from the analysis of the μ_0 data a small fraction φ of the DEH population must exist as rapid-reactive DEH^r states to successfully account for the deduced IND(*t*) dynamics. This conclusion is again illustrated in Figure 6 where it is observed that the absence of such DEH^r states (φ = 0) would result in an exactly linear dependence of IND(*t*) (= *I*(*t*)) across the entire range of experimental UV exposure. Conversely, a highly non-linear IND(*t*) response is expected within the experimental UV exposure period for φ = 1 as complete IND conversion becomes possible and N_t approaches saturation. The necessity to introduce rapid-reacting DEH^r states (φ ≠ 0) into the dynamic model is thus simply a consequence of the inherently low oxygen reaction rate with DEH^b states under the original assumption that ε >> 1. The reaction rate (=$4\pi\rho_R DC$ from Equation (5e)) is inherently controlled by the magnitude of the oxygen diffusion coefficient and the decay of induced radical states via diffusion-reaction kinetics may usefully be analysed to determine oxygen diffusion coefficients in polymer materials under specified boundary conditions [22,23]. The magnitude of the oxygen diffusion coefficient that is appropriate for the present MDP films is uncertain but assuming that C_{sol} is comparable to the pure PET

magnitude (~ 5×10^{17} cm^{-3} from PET solubility coefficients [24]) the deduced diffusion coefficient for the present MDP films is about 2×10^{-16} $cm^2 \cdot s^{-1}$. The magnitude of this diffusion coefficient is considerably lower than that reported for pure PET ($D \sim 4 \times 10^{-9}$ $cm^2 \cdot s^{-1}$ [23,24]) but may reflect an increase in the effective size of the penetrant O_2 molecules due to the presence of the DEH dopant. This apparently low value for D may have associated implications for the ability of atmospheric oxygen to replenish consumed oxygen throughout the UV absorption depth since this will require a time $\sim \alpha^{-2}/D = 10^6$ s which is comparable to the maximum experimental exposure time. Such oxygen starvation effects do not appear to be manifest in the inferred trap generation magnitudes, however, which greatly exceeds the value for C_{sol}. The available concentration of soluble oxygen would therefore appear to be maintained at around the solubility limit throughout the entire exposure period but is unable to diffuse and react efficiently with excited DEH^b states before they relax to DEH. It is noted that the alternative scenario, whereby D remains comparable to the pure PET magnitude with $\varepsilon << 1$, would require that the DEH^b reaction rate was highly inefficient ($<10^{-6}$) to account for the observed trap generation dynamics. This is inconsistent with independent estimates of the DEH to IND conversion efficiency which is reported to be as high as 0.4 [13] and is in fact more typical of the envisaged DEH^r reaction process discussed below.

The preceding considerations concerning relaxation and reaction of DEH^b states afford additional insight into the possible nature of the counterpart DEH^r states. It is first noted that the DEH^r states cannot simply represent a subset of DEH^b states which are effectively stable ($\beta = 0$) and subsequently react with soluble oxygen, via the same diffusive-reaction kinetics for DEH^b states, even after UV exposure has been terminated. The existence of such stable states would imply that the eventual conversion to indazole, and its experimental detection, might be sensitive to the timescale when post-exposure TOF and SCLC measurements are performed but such evidence is absent from a survey of the sample handling history. The DEH^r states must consequently represent sites within the MDP where oxygen is immediately available to initiate the indazole reaction. Such sites could therefore represent a proportion of micro-void regions within the polymer where the movement of oxygen is unrestricted by diffusion. However, for the present MDP films the interpretation of the fitted parameter φ (= 0.01) would then require that the observed saturated indazole concentration should not exceed $\varphi M_0 = 10^{19}$ cm^{-3} which is clearly violated from the data in Figure 5. The parameter φ would thus appear to represent the fraction of DEH states which, upon excitation by UV irradiation, lie within the reaction radius of soluble oxygen molecules and are immediately converted to indazole. For this scenario, φ may be estimated by considering the ratio of the average volume V(DEH) that is occupied by an excited DEH state to the average volume $V(O_2) \sim C_{sol}^{-1}$ occupied by a soluble oxygen molecule. For small φ V(DEH) is dominated by DEH^b states so that $V(DEH) \sim B^{-1}$ which changes dynamically with UV exposure time (Figure 4). Restricting attention to the time regime where $B(t)$ is approximately constant $V(DEH) \sim \left(\overline{G} M_0 / \beta\right)^{-1}$ from Equation (5b) and the quantity φ may thus be expressed as:

$$\varphi \approx \beta C_{sol} / \overline{G} M_0 \tag{10}$$

For the parameters employed to generate the model curves in Figures 4–6, Equation (10) produces an a priori calculated value for $\varphi = 0.004$ which shows reasonable agreement with the (average) 0.01 value deduced by data fitting across the entire exposure period.

Using the insight gained regarding the apparent dominance of DEH^r states in generating IND traps it is finally possible to consider what restrictions should be imposed upon the supply of oxygen in the MDP bulk to minimise degradation of the electronic performance of the MDP films over operationally long UV exposure periods. It is helpful in this respect to realise that the φ expression in Equation (10) may be used in Equation (9) to produce a revised expression for IND(t) whereby:

$$IND(t) = M_0\left[1 - e^{-\left(\frac{C_{sol}}{M_0}\right)\beta t}\right] \tag{11}$$

This expression embodies the principal IND trap generation kinetics via DEH^r states and confirms a number of key characteristics that have emerged from the more detailed modeling using the partial differential rate equations. A perhaps surprising parameter to appear in Equation 11 is β as this would intuitively be associated with DEH^b processes (Equation (5b)). However, β also influences the concentration of DEH states according to Equation (5a) which in turn controls the concentration of UV excited DEH^r states via Equation (5c). The overall rate of IND(t) production should thus be enhanced for larger β as confirmed in Equation (11). The rate of IND(t) production is also predicted to depend upon the ratio of C_{sol} to M_0 which is again physically compatible with the proposed DEH^r reaction model which should become more efficient as the availability of soluble oxygen becomes comparable to the overall DEH concentration.

For any given MDP film, Equation (11) suggests that there are consequently very few experimental parameters that may be engineered to slow the rate of IND(t) trap generation. M_0 is specified by the selected C_w for the MDP doping, and β is presumably characteristic of molecular electronic interactions between the dopant-polymer constituents. Only C_{sol} may therefore be experimentally controlled which in practice would require the use of a vacuum coating system to initially desorb soluble oxygen from the films before an encapsulation layer is deposited to restrict re-absorption of oxygen upon return to atmospheric pressure. Such an encapsulation strategy would be critically dependent upon the encapsulation layer preventing the soluble oxygen concentration from re-attaining its pre-desorption level. The ability to maintain desorbed oxygen levels at a fractional level of their initial C_{sol} magnitude not only reduces the rate of IND(t) increase as indicated by Equation (11) but significantly would also restrict the maximum IND concentration that may eventually be generated as the finite supply of soluble oxygen is entirely consumed in photo-cyclic reactions. Significant extension of the operational lifetime of the MDP films may therefore be possible but difficult to achieve using standard thin-film coating technologies.

It is curious to note that UV shielding of the exposed MDP surface is not apparently predicted to afford better protection against DEH^r photo-degradation effects according to Equation (11). This incorrect interpretation arises through the substitution of the $\varphi\overline{G}$ product in the exponent term of Equation 9 with the constant parameters from Equation (10). As the UV generation rate $\overline{G}$ is reduced, however, φ will increase but is restricted to a maximum value of unity. A reduction in the rate of IND(t) production will consequently be achieved for UV generation rates that fall below a magnitude $\beta C_{sol}/M_0$ which for the present MDP parameters would require a reduction in the UV incident photon flux by a factor >100. Shielding may not therefore be pragmatic if the MDP layer is to be deployed in an optoelectronic application which demands a UV spectral response.

4. Conclusions

The degradation of hole transport properties in DEH doped polyester films upon UV irradiation is consistent with the photo-cyclic conversion of DEH to IND molecules which function as hole traps. The generation dynamics of the IND traps is found to be dominated by the photo-stimulation of DEH^r states which lie within the reaction radius of soluble oxygen and rapidly convert to indazole before relaxation to DEH may occur. Around 1% of all DEH excitation events must produce DEH^r states for the experimental UV photon flux employed to provide a consistent quantitative fit to the electronic degradation effects observed in TOF and SCLC data. The parameters deduced from the trap generation dynamics suggest that encapsulation strategies to restrict the supply of soluble oxygen, and thereby minimise MDP degradation effects, would be effective but difficult to implement.

Acknowledgments

The author acknowledges access to industrial coating equipment to allow fabrication of the samples.

Conflicts of Interest

The author declares no conflict of interest.

References

1. Street, R.; Wong, W.; Ready, S.; Chabinyc, I.; Arias, A.; Limb, S.; Salleo, A.; Lujan, R. Jet printing flexible displays. *Mater. Today* **2006**, *9*, 32–37.
2. Makela, T.; Jussila, S.; Kosonen, H.; Backlund, T.; Sandberg, H.; Stubb, H. Utilizing roll-to-roll techniques for manufacturing source-drain electrodes for all-polymer transistors. *Synth. Met.* **2005**, *153*, 285–288.
3. Kololuoma, T.; Tuomikoski, M.; Makela, T.; Heilmann, J.; Haring, T.; Kallioinen, J.; Hagberg, J.; Kettunen, I.; Kopola, H. Towards roll-to-roll fabrication of electronics, optics and optoelectronics for smart and intelligent packaging. *Proc. SPIE* **2004**, *5363*, 77–85.
4. Giannouli, M.; Drakonakis, V.M.; Savva, A.; Eleftheriou, P.; Florides, G.; Choulis, S.A. Methods for improving the lifetime performance of organic photovoltaics with low-costing encapsulation. *Chem. Phys. Chem.* **2015**, *16*, 1134–1154.
5. Goldie, D.M. Organic Charge Transport Materials for Xerographic Imaging. In *Handbook of Photochemistry and Photobiology*, Nalwa, H.S., Ed.; American Scientific Publishers: Valencia, CA, USA, 2003; Volume 2, pp. 195–256.
6. Mack, J.X.; Schein, L.B.; Peled, A. Hole mobilities in hydrazone-polycarbonate dispersions. *Phys. Rev. B* **1989**, *39*, 7500–7508.
7. Schein, L.B.; Rosenberg, A.; Rice, S.L. Hole transport in a molecularly doped polymer-p-diethylaminobenzaldehyde-diphenylhydrazone in polycarbonate. *J. Appl. Phys.* **1986**, *60*, 4287–4292.
8. Borsenberger, P.M.; Fitzgerald, J.J. Effects of the dipole-moment on charge transport in disordered molecular-solids. *J. Phys. Chem.* **1993**, *97*, 4815–4819.

9. Kanemitsu, Y.; Imamura, S. Photocarrier generation, injection, and trapping at the interface in a layered organic photoconductor-metal-free phthalocyanine molecularly doped polymer. *J. Appl. Phys.* **1990**, *67*, 3728–3736.
10. Sasvari, G.; Juhasz, C. A study of molecularly doped polymer-to-metal contacts by steady state injection current measurements. *J. Phys. Condens. Matter* **1997**, *9*, 6493–6503.
11. Pacansky, J.; Coufal, H.C.; Brown, D.W. The photocyclization of a hydrazone to an indazole. *J. Photochem.* **1987**, *37*, 293–313.
12. Pacansky, J.; McLean, A.D.; Miller, M.D. Theoretical calculations and experimental studies on the electronic structures of hydrazones and hydrazone radical cations: Formaldehyde hydrazone and benzaldehyde diphenylhydrazones. *J. Phys. Chem.* **1990**, *94*, 90–98.
13. Stasiak, J.W.; Storch, T.J. Hole mobilities in photochemically modified DEH-doped polycarbonate. *J. Imaging Sci. Technol.* **1996**, *40*, 299–303.
14. Srivistava, A.; Singh, V.; Aggarwal, P.; Schneeweiss, F.; Scherer, U.W.; Friedrich. W. Optical studies of insulating polymers for radiation dose monitoring. *Indian J. Pure Appl. Phys.* **2010**, *48*, 782–786.
15. Prasad, S.G.; De, A.; De, U. Structural and optical investigations of radiation damage in transparent PET polymer films. *Int. J. Spectrosc.* **2011**, *2011*, 1–7.
16. Pautmeier, L.; Richert, R.; Bassler, H. Anomalous time-independent diffusion of charge-carriers in a random potential under a bias field. *Philos. Mag. B* **1991**, *63*, 587–601.
17. Borsenberger, P.; Pautmeier, L.; Bassler, H. Charge transport in disordered molecular-solids. *J. Chem. Phys.* **1991**, *94*, 5447–5454.
18. Mort, J.; Pfister, G.; Grammatica, S. Charge transport and photogeneration in molecularly doped polymers. *Solid State Commun.* **1976**, *18*, 693–696.
19. Lampert. M.; Mark, P. *Current Injection in Solids*; Academic Press: New York, NY, USA, 1970.
20. Goldie, D.M. Interface controlled current injection in hydrazone doped polyesters. *Thin Solid Films* **2010**, *519*, 1391–1396.
21. Szymanski, M.Z.; Kulszewicz-Bajer, I.; Faure-Vincent, J.; Djurado, D. Comparison of simulations to experiment for a detailed analysis of space-charge-limited transient current measurements in organic semiconductors. *Phys. Rev. B* **2012**, *85*, doi:10.1103/PhysRevB.85.195205.
22. Vyazovkin, V.L.; Korolev, V.V.; Syutkin, V.M.; Tolkatchev, V.A. On oxygen diffusion in poly(methyl methacrylate) films. *React. Kinet. Catal. Lett.* **2002**, *77*, 293–299.
23. Rharbi, Y.; Yekta, A.; Winnik, M. A method for measuring oxygen diffusion and oxygen permeation in polymer films based on fluorescence quenching. *Anal. Chem.* **1999**, *71*, 5045–5053.
24. Serad, G.E.; Freeman, B.D.; Stewart, M.E.; Hill, A.J. Gas and vapour sorption and diffusion in poly(ethylene terphthalate*). Polymer* **2001**, *42*, 6929–6943.